

**INVESTIGATION OF ELECTRICAL RESISTANCE SPOT  
WELDING USING FINITE ELEMENT ANALYSIS**

**ELEKTRİK DİRENÇ PUNTA KAYNAĞININ SONLU  
ELEMENLAR ANALİZİ İLE İNCELENMESİ**

**ALPEREN YETKİN**

**ASST. PROF. DR. MEHMET OKAN GÖRTAN**

**Supervisor**

Submitted to  
Graduate School of Science and Engineering of Hacettepe University  
as a Partial Fulfillment to the Requirements  
for the Award of the Degree of Master of Science  
in Mechanical Engineering.

2024

## **ABSTRACT**

# **INVESTIGATION OF ELECTRICAL RESISTANCE SPOT WELDING USING FINITE ELEMENT ANALYSIS**

**Alperen YETKİN**

**Master of Science, Department of Mechanical Engineering**

**Supervisor: Asst. Prof. Dr. Mehmet Okan GÖRTAN**

**September 2024, 33 pages**

The resistance spot welding is widely used in industry especially in automotive industry where the trend is ultra-high strength steels. Since the experimental testing methods are costly, computer-aided numerical methods are essential for quickly and cost effectively identify optimum parameters in RSW. In this thesis, resistance spot welding of ultra-high strength steel MS1500 will be investigated from various aspects using electro-thermo-mechanical coupled finite element analysis. The expulsion limits and optimal nugget growth parameters obtained from finite element analysis will be compared with experimental results. Additionally, the effect of temperature change rates resulting from the resistance spot welding process will be examined.

**Keywords:** Resistance Spot Welding, Ultra High Strength Steel, UHSS, MS1500, Finite Element Analysis, FEA.

# ÖZET

## ELEKTRİK DİRENÇ PUNTA KAYNAĞININ SONLU ELEMENLAR ANALİZİ İLE İNCELENMESİ

**Alperen YETKİN**

**Yüksek Lisans, Makina Mühendisliği Bölümü**

**Tez Danışmanı: Dr. Öğr. Üyesi Mehmet Okan GÖRTAN**

**Eylül 2024, 33 sayfa**

Elektrik direnç nokta (punto) kaynağı, özellikle ultra yüksek mukavemetli çeliklerin giderek trend olduğu otomotiv sektöründe yaygın olarak kullanılmaktadır. Deneysel test yöntemlerinin maliyetli olması nedeniyle, bilgisayar destekli sayısal yöntemler, direnç nokta kaynağında optimum parametrelerin hızlı ve maliyet etkin bir şekilde belirlenmesi için kritik öneme sahiptir. Bu tezde, ultra yüksek mukavemetli çelik olan MS1500'ün nokta direnç punto kaynağı, elektro-termo-mekanik bağlı sonlu elemanlar analizi kullanılarak birçok açıdan incelenecektir. Sonlu elemanlar analizi ile elde edilen sıçrama sınırları ve ideal kaynak çekirdeği oluşma parametreleri, deneysel sonuçlarla karşılaştırılacaktır. Ayrıca, kaynak işlemi nedeniyle meydana gelen sıcaklık değişim hızlarının etkisi de incelenecektir.

**Anahtar Kelimeler:** Direnç Nokta Kaynağı, Punto Kaynağı, Ultra Yüksek Dayanımlı Çelikler, MS1500, Sonlu Elemanlar Analizi.

## ACKNOWLEDGEMENTS

I would like to express my deepest gratitude to my thesis advisor, Assist. Prof. Dr. Mehmet Okan GÖRTAN, for his invaluable guidance, support, constructive feedback, and patience, which have been crucial to the successful completion of my studies.

I am profoundly grateful to my wife, Gülşah TÜFEKÇİOĞLU YETKİN, for her enduring patience, understanding, and encouragement throughout this journey. Her support has been a constant source of strength and motivation.

Special thanks to my friend Kemal Can SARI for his invaluable assistance and for always being there to offer support and perspective.

Finally, I wish to acknowledge my family-my father, Taner; my mother, Ümmühan; and my sister, Fatma-for their constant love, encouragement, and belief in me. Their support has been invaluable in every aspect of my life.

# TABLE OF CONTENTS

ABSTRACT .....	i
ÖZET .....	ii
ACKNOWLEDGEMENTS.....	iii
TABLE OF CONTENTS .....	iv
LIST OF FIGURES .....	v
LIST OF TABLES .....	vi
ABBREVIATIONS.....	vii
1. INTRODUCTION .....	1
2. STATE OF THE ART.....	3
2.1. AHSS-UHSS Definitions .....	3
2.2. Resistance Spot Welding .....	4
2.3 Finite Element Model of RSW .....	6
3. MATERIAL AND METHODOLOGY .....	9
3.1. MS1500 UHSS Properties .....	9
4. RESULTS AND DISCUSSION .....	16
5. SUMMARY AND OUTLOOK .....	25
6. REFERENCES .....	26
APPENDIX .....	29
Appendix 1 – Marc Unit System (millimetre based) .....	29
Appendix 2 – Material Properties of MS1500 and Contact Parameters .....	31
Appendix 3 – Thesis Originality Report.....	34
AUTHOR BIOGRAPHY .....	35

## LIST OF FIGURES

<b>Figure 2.1.</b> Global Formability Diagram 2021 (banana diagram) – World Auto Steel .....	4
<b>Figure 2.2.</b> Schematic representation of RSW .....	5
<b>Figure 2.3.</b> Typical RSW process graph .....	5
<b>Figure 3.1.</b> Mechanical Properties of MS1500 Steel (See Appendix 2 for tabular values) .....	10
<b>Figure 3.2.</b> Physical Properties of MS1500 (See Appendix 2 for tabular values) .....	11
<b>Figure 3.3.</b> Finite Element Model of RSW Process .....	12
<b>Figure 3.4.</b> Process parameters (Force and 10 Cycle Current w.r.t. Time) .....	12
<b>Figure 3.5.</b> AC Current Application on RSW .....	13
<b>Figure 3.6.</b> Change of Contact Electrical Conductivity w.r.t Temperature (See Appendix 2 for tabular values).....	14
<b>Figure 4.1.</b> Comparison of Experimental and FEA Results of RSW Process with 8 kA Current and 3.4 kN of Force .....	16
<b>Figure 4.2.</b> Schematic Representation of the Experiment of Shear Breaking on Welded Joint to Investigate the Expulsion Occurrence. ....	18
<b>Figure 4.3.</b> Expulsion Comparison of Experimental and FEA Results of RSW process with 9 kA current and 3.4 kN of force .....	19
<b>Figure 4.4.</b> Expulsion Comparison of Experimental and FEA Results of RSW process with 10 kA current and 3.4 kN of force .....	20
<b>Figure 4.5.</b> Identification of nodes whose temperatures are examined in the analysis .....	21
<b>Figure 4.6.</b> Temperature data of the selected nodes during current application in the analysis .....	22
<b>Figure 4.7.</b> Temperature data of the selected nodes after current application in the analysis .....	23

## LIST OF TABLES

<b>Table 3.1.</b> Chemical Composition of MS1500 [wt.%] .....	9
<b>Table 3.2.</b> Mechanical Properties of MS1500 .....	9
<b>Table 3.3.</b> Temperature independent material properties on model .....	9
<b>Table 3.4.</b> Contact Properties Defined on Model.....	14
<b>Table 4.1.</b> Nugget dimensions of test samples and FEA results .....	17
<b>Table 4.2.</b> Temperature change rate on different time intervals of selected nodes.....	24

## ABBREVIATIONS

AHSS	Advanced High Strength Steels
AISI	American Iron and Steel Institute
CALPHAD	Calculation of phase diagram
DP	Dual Phase (Steel)
FDM	Finite Difference Method
FEA	Finite Element Analysis
ISO	International Organization for Standardization
LME	Liquid Metal Embrittlement
MS	Martensitic
RSW	Resistance Spot Welding
TRIP	Transformation Induced Plasticity (Steel)
UHSS	Ultra High Strength Steels

# 1. INTRODUCTION

Automobile industry has been under constant pressure to reduce weight of the passenger cars for the last two decades due to the tightening in greenhouse gas emission regulations. These restrictive emission rules are becoming more challenging for manufacturers with each passing year. Vehicle weight has a substantial effect on passenger cars fuel consumption and thus on emissions. Therefore, the automobile industry is in constant search for lightweight materials. Thanks to their very high strength to density ratio combined with low cost, compatibility with the welding process and acceptable level of formability, ultra-high strength steels (UHSS) have become the material of choice [1]. However, with the development of new material technologies, appropriate joining strategies should also evolve.

Thanks to its good repeatability and high production rate, resistance spot welding (RSW) is the preferred joining process especially in the automotive industry. Each passenger car incorporates multiple thousand resistance spot welded joints [2]. During the RSW process, heat is generated directly in the faying section of the joint due to the contact and material bulk resistance against current which flows through them.

During the RSW process, heating occurs according to joule law and is linearly proportional to the square of the applied current, total resistance of the sheets to be joint and the welding time [3]. Material melts and generates a fusion section called as nugget. Among others, nugget size is the main parameter which affects weld strength and quality. As welding time and current increase, nugget size also grows. However, squirting of the liquid metal out of the fusion zone, which is called as expulsion is the limiting factor of welding current and time. Expulsion has deteriorating effects on RSW joint's strength and should be therefore avoided [3]. Thus, welding process parameters should be selected appropriately. Despite the primary focus on key process parameters such as welding current and time, it is essential to recognize that the success of the RSW process is profoundly influenced by factors beyond these, including heat transfer to the environment and alterations in physical properties of materials in response to temperature rise. Moreover, the consequential deformation within the fusion zone also plays a crucial role in determining the overall quality of the RSW process [4].

Hence, thorough testing is required to find optimum welding parameters which are costly and require a significant amount of time. In order to avoid time-consuming testing, finite element analysis methods can be utilised. However, due to the nature of the process, electro-thermo-mechanical coupled analysis is required which necessitates correct selection of thermal, physical and mechanical properties of the used materials.

In this study, the RSW joining process of UHSS MS1500 material is investigated using non-linear electro-thermo-mechanically coupled finite element simulations and numerical results are validated with experiments.

## 2. STATE OF THE ART

### 2.1. AHSS-UHSS Definitions

Advanced High Strength Steel (AHSS) refers to a group of high-strength steel alloys that undergo advanced heat treatment processes to achieve superior mechanical properties. AHSS typically exhibits tensile strengths exceeding 550 MPa, with some specialized grades reaching up to 1000 MPa. These steels offer a combination of high strength, excellent formability, and enhanced crash performance compared to conventional steel grades. AHSS facilitates significant weight reduction while maintaining structural integrity, making it indispensable especially in automotive applications.

Within the spectrum of AHSS, a subset known as Ultra High Strength Steel (UHSS) emerges, elevating the standards of strength, resilience, and performance to unprecedented levels. Although there is no exact and accepted definition, the UHSS class generally covers steels with a tensile strength of over 1000 MPa. This powerful class of steel finds its niche in applications demanding uncompromising strength-to-weight ratios. Martensitic (MS) steels belong to that class and are produced from the austenite phase by rapid quenching to transform most of the austenite to martensite. The MS steels are characterized by a martensitic matrix containing small amounts of ferrite and/or bainite. [5]

The integration of high-strength martensitic UHSS has revolutionized vehicle design approaches in the automotive sector, facilitating substantial weight reduction while enhancing crashworthiness and occupant safety. By utilizing the exceptional mechanical properties of martensitic UHSS, automotive manufacturers achieve extraordinary levels of structural integrity, leading to superior performance and enhanced fuel efficiency. Particularly, the usage of Ultra High Strength Steel (UHSS) in impact beams has become extensive [2]. Moreover, AHSS finds prevailing application in various structural and chassis components, further underlining its significance in modern automotive engineering [2].

The steel global formability diagram also called banana diagram, a graphical representation of the forming limit curve, serves as a valuable tool in clarifying the relationship between strength and formability in AHSS and UHSS. This diagram, shown in Figure 2.1., provides a visual depiction of the trade-off between tensile strength and

elongation, aiding material scientists and engineers in optimizing material selection and forming processes for various applications.

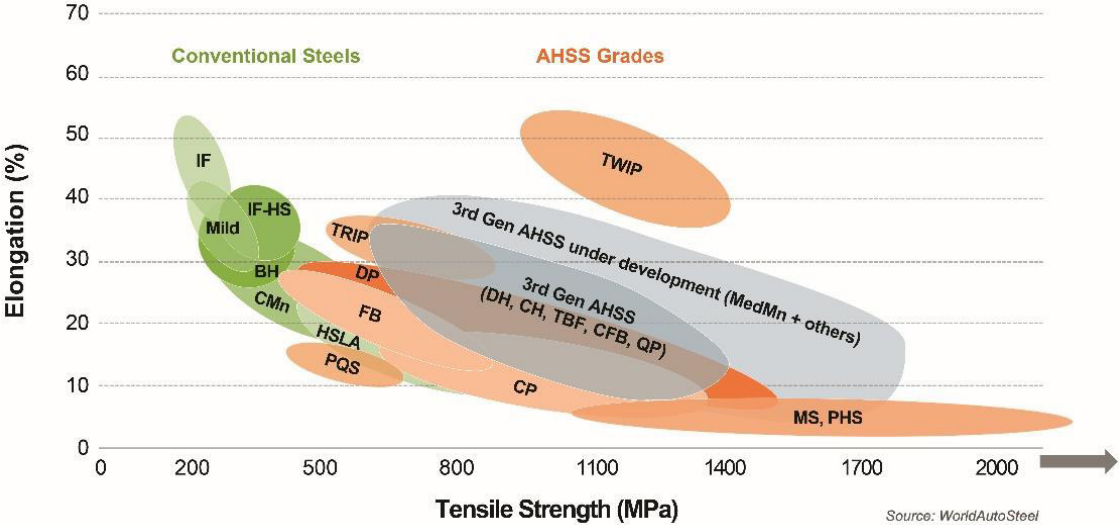


**Figure 2.1.** Global Formability Diagram 2021 (banana diagram) – World Auto Steel

Thanks to its exceptional strength levels, coupled with remarkable formability and manufacturability, UHSS allows the creation of lightweight and durable components, which are essential for evolving demands of a rapidly changing world.

**2.2. Resistance Spot Welding**

Welding is the process of joining two or more parts together using heat, pressure or both, resulting in a unified structure. Resistance welding relies on the heat generated by the resistance of workpieces and their contacting surfaces when an electrical current passes through. Spot welding is the most widely used example of lap joining, executed through shaped electrodes that remain stationary during the welding process.

The applied force presses the surfaces of the sheets into initial contact. Then current is passed through the electrodes and work sheets for a short time. The electrode faces concentrate the welding current into a small spot which results in high temperature spot to be melted. The schematic representation of RSW illustrated in Figure 2.2.

The heat is obtained by Joule Effect, and the pressure is provided by pressing the electrodes towards each other. The heat causes a molten zone in the assembly and turns into welded joint after the solidification under pressure. Since steel has relatively high electrical resistance, its easily heats up with the current flow and therefore is an ideal metal alloy for resistance spot welding. [6]

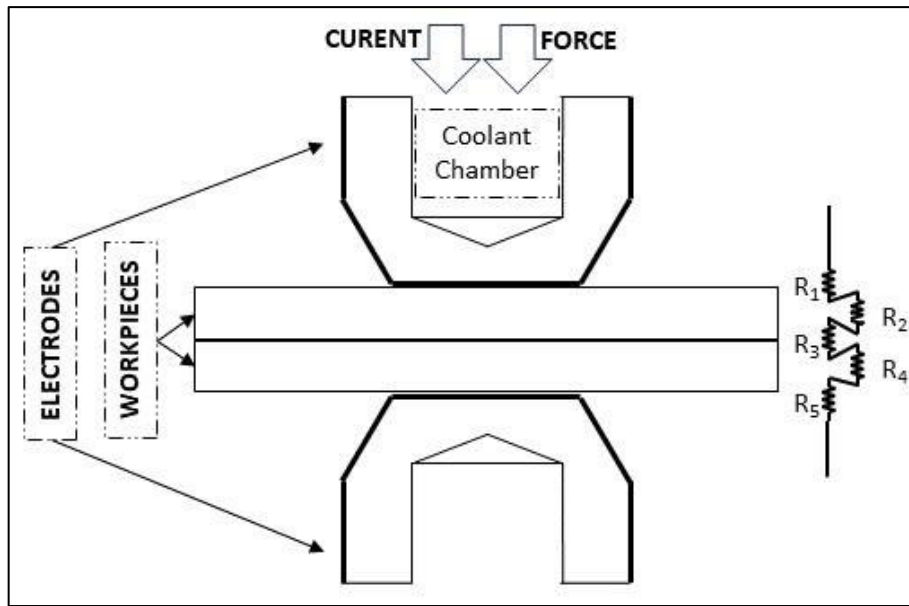


**Figure 2.2.** Schematic representation of RSW

$R_1$  and  $R_5$  are electrical contact resistance between electrode and workpiece,  $R_2$  and  $R_4$  are bulk resistance of workpieces,  $R_3$  is the contact resistance between workpieces on Figure 2.2.

The resistance spot welding method offers the capability to weld multiple sheets as long as the correct electrode type and dimensions, as well as appropriate force and current settings are provided. Basic steps of the process shown on Figure 2.3. The main controlled output is dimensions of the nugget, which significantly influence weld quality.

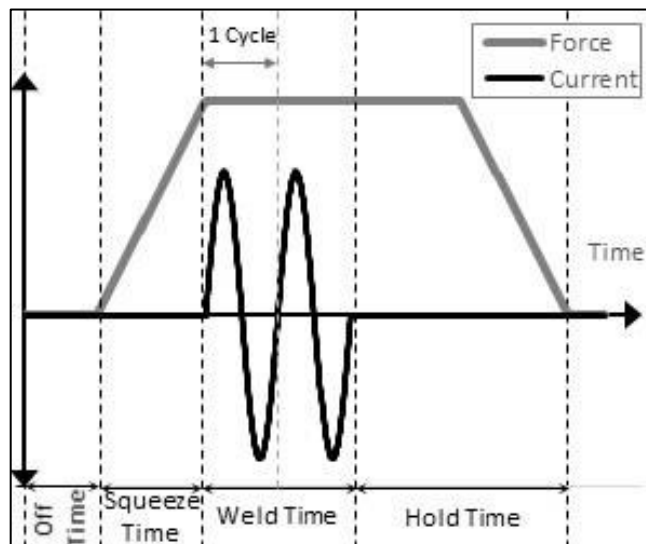


**Figure 2.3.** Typical RSW process graph

At elevated current levels, expulsion occurs, involving the forceful ejection of molten metal from between the sheets. While welds with minor expulsion are typically acceptable, excessive expulsion is undesirable due to its tendency to introduce inconsistencies.

### **2.3 Finite Element Model of RSW**

Finite element analysis (FEA) is a widely used simulation method in engineering and science. It is used to model the behaviour of complex structures or processes using a computer-based approach. FEA is utilized to predict the responses of structures under various loads or process outputs of various inputs. The RSW process can be simulated using FEA in a variety of methods.

Both electrical and mechanical aspects are fundamental inputs in the RSW process. Electrical input subsequently triggers the involvement of thermal aspects, as the heat generated by electrical resistance due to the physical properties and contact geometry. Contact geometry also changes with the applied force and the mechanical properties of the material which is also temperature dependent. Therefore, for accurate results with realistic models, it is necessary to handle all three types of analyses, namely electrical, thermal and mechanical. Early studies were conducted in a manner that involved electro-thermal and thermo-mechanical coupling, where the outcomes of electro-thermal coupled analysis served as inputs for thermo-mechanical coupled analysis. Modern studies are carried out with electro-thermo-mechanical coupled analyses thanks to software and hardware advances.

Electrical-thermal-mechanical coupled simulations are essential for analysing RSW due to its nature. Furthermore, it is observed that resistance welding applications often demonstrate geometrically axisymmetric properties. Taking advantage of this geometrical characteristic in the FEA models can be beneficial for performing analysis calculations.

Although the numerical solution methods used to predict the behaviour in RSW dating back to 1960s, they were only focusing to the electro-thermal behaviour of the process. Archer [7] and Greenwood [8] created numerical models to predict nugget growth with temperature independent material properties. Archer used one-dimensional model while Greenwood created an axisymmetric numeric model to investigate temperature variations on the fusion zone. Also, the contact resistance neglected on these studies which highly

affects the result because RSW generally applies on thin metal sheets. The contact resistance gets more significant as the workpieces gets thinner which decreases their bulk resistance while the contact resistance remains almost same.

Since nugget growth is highly depending on the heat generated both by the materials bulk resistance and by the contact surface, Nied [9] established a mechanical model to determine the contact surface of the workpieces, enabling to couple the electro-thermal numeric solution. Despite utilizing elastic equations, with this electro-thermo-mechanical coupled axisymmetric model, it became feasible to investigate the formation of weld nuggets.

To create a FEA model of RSW process, temperature dependent material properties are needed. Also, contact properties like heat transfer coefficients, electrical resistivity should be properly defined in the model. The resultant electrical resistivity of the material bulk resistance and the contact resistance of faying surface is determining the heat generated with the amount of current. Due to this heat energy, the temperature values at the nodes of the elements are updated and mechanical part of the analysis takes place after the material mechanical properties changed with temperature. New contact area is calculated within mechanical part of the analysis.

Tsai took it one step further and develop a RSW model to investigate type 347 stainless steel and AISI1045 carbon steel with thermo-electric, iso-parametric and surface element types [10]. The study includes electro-thermo-mechanical coupled analysis by integrating these 3 types of elements and the resistance on the faying surface is modelled temperature dependent as well as the material thermal-mechanical properties.

Later on, Eisazadeh et al. investigated RSW process on AISI 1008 steel with and axisymmetric electro-thermo-mechanical coupled model [11]. The study focused on effect of variation of each process parameters on the weld quality. The study also includes the comparison with both the one-dimensional model and the experimental data from literature.

Nielsen et al. studied welding DC06 low carbon steel with 2 thicker AHSS (DP600 and TRIP700) and HSLA 340 steels by both numerical model and experiments [12]. Due to the good correlation between experimental results and numerical models, they indicated that FEA is a valuable tool in the optimization of the RSW process for triple layered AHSS.

Afterward, Zheng et al. studied to optimize RSW parameters on between UHSS and mild steels by building coupled axisymmetric finite element model [13]. The study includes these dissimilar types of steels because the predominant use of mild steel automotive body despite the utilization of UHSS in some specific regions where high strength required.

Andersson and Melander performed simulation of RSW with 6 steel types including UHSS with FEA [14]. The study includes the comparison of the nugget size as well as the expulsion occurrence limit investigation. It's also examined that the deviations between the results of finite element analysis and the experiments on the nugget size arising from the shunting effect, resulting from the application of welding processes from two separate points on the same workpieces in the study. The FE model created with a software that specifically designed for simulate welding for commercial use.

Hoang Li et al established a CALPHAD (Calculation of phase diagram)-coupled FEM model to investigate crack formation mechanism during liquation and solidification phases in RSW of 7075 and 6061 aluminium alloys [15].

Liquid Metal Embrittlement (LME) in RSW examined by Hideki Ueda et al. [16] and Wook-Sang Jeon et al. [17] with FEA simulations. Ueda focused on the influence of clearance between steel plate and electrode on crack initiation in corona bonds with his FEA model. Jeon conducted an analysis into the causes of LME during the RSW in the galvanized TRIP steels, type of AHSS, with finite element model.

Mehdi Jafari et al. published an article about review FEA of RSW, which he compares the FDM and FEA methods for investigating RSW. Jafari highlights temperature dependent electrical and thermal contact properties are the most effective parameters on the FEA models because of great effect on the RSW process simulations. [18]

In addition, when examining other welding methods with FEA apart from RSW, the heat input is generally calculated independently from the analysis and then integrated into the model. B. Yildirim and H.F. Nied developed a model to analyze and predict transient temperature profiles, residual stresses and distortion incurred during deposition of protective overlay. In the model, heat input from the weld torch is applied as a distributed surface heat flux during each weld pass.[19]

### 3. MATERIAL AND METHODOLOGY

#### 3.1. MS1500 UHSS Properties

This study focused on the simulation of RSW on MS1500 martensitic steel. Chemical composition of the material shown on Table 3.1. The remarkably high strength of this material mainly from the heat treatment, pre-forming processes and from alloying elements. Basic mechanical properties of MS1500 shown on Table 3.2.

**Table 3.1.** Chemical Composition of MS1500 [wt.%]

C	Si	Mn	P	S	Al	Ti	Cr	Mo	B	Cu
0.210	0.215	1.080	0.007	0.003	0.043	0.030	0.025	0.009	0.002	0.103

**Table 3.2.** Mechanical Properties of MS1500

Yield Strength [MPa]	Tensile Strength [MPa]	Total Elongation [%]
1455,7 ± 41,7	1616,1 ± 2,2	5,55 ± 0,49

FEA performed on the MSC Marc-Mentat software. At the pre-processing stage, material properties are added to the software. Since the analysis is performed electro-thermo-mechanical coupled (analysis type on software: current / thermal / structural), mechanical thermal and electrical properties have to be defined. Considering the temperature changes are very high on the RSW process, mechanical and electrical properties should be defined as temperature dependent.

In the RSW simulation, mass density, thermal expansion coefficient and the Poisson's ratio are defined temperature independent, and values used on model shown on Table 3.3., even though they are, for the calculations to converge.

**Table 3.3.** Temperature independent material properties on model

Mass Density [kg/m <sup>3</sup> ] – [t/mm <sup>3</sup> ]*	Thermal Expansion Coeff. [1/°K]	Poisson's Ratio (unitless)
7850 – 7.85E-09	1.46E-05	0.29

\*: Unit used in MSC Marc “Milimeter” based system. See Appendix 1 for consistent system of units Table for the MSC Marc model.

Exact values of material properties for MS1500 with respect to temperature are not available in the literature. Required material properties are defined to the model with assumptions.

Young’s Modulus of the MS1500 values with respect to temperature is derived from DP1000 steel properties [20][21] and shown in Figure 3.1.

As a plasticity property of the MS1500, yield strength is defined linearly decreasing as the temperature increases from 300 K° to 1000 K°. Values of the yield strength with respect to temperature used on FEA model shown in Figure 3.1.

Once the yield strength reaches as low as 30 MPa, it is assumed to remain nearly constant to allow the simulation to continue calculating while the material melts. In reality, its yield strength approaches nearly 0 MPa above 1700 K°, because the material undergoes melting.

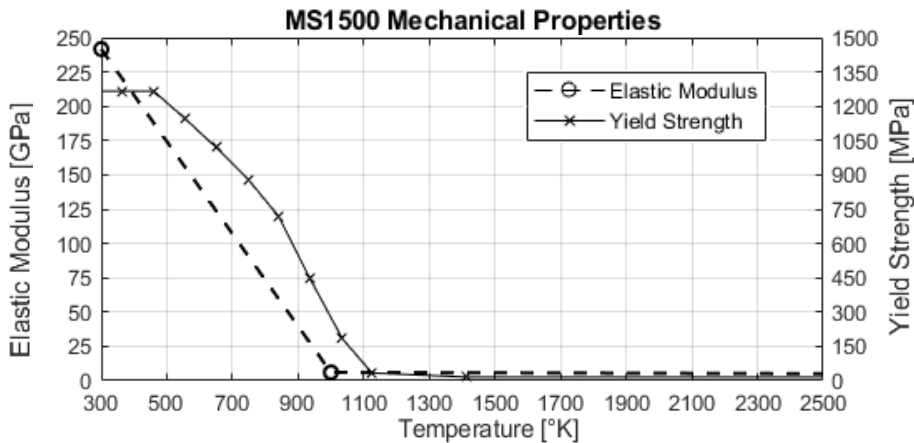


**Figure 3.1.** Mechanical Properties of MS1500 Steel (See Appendix 2 for tabular values)

Thermal conductivity and the specific heat capacity have been assumed to match those of DP600 steel [21] and defined as temperature dependent shown in Figure 3.2.

Due to limited availability of temperature dependent data in the literature, electrical resistivity property of the MS1500 have been assumed to be similar to 4140 alloy [22], based on akin chemical composition. The available data for temperatures ranging from 300 to 870 °K have been extrapolated using third-degree polynomial fitting to extend the range up to 2600 °K. Values of the resistivity used on FEA model shown in Figure 3.2.

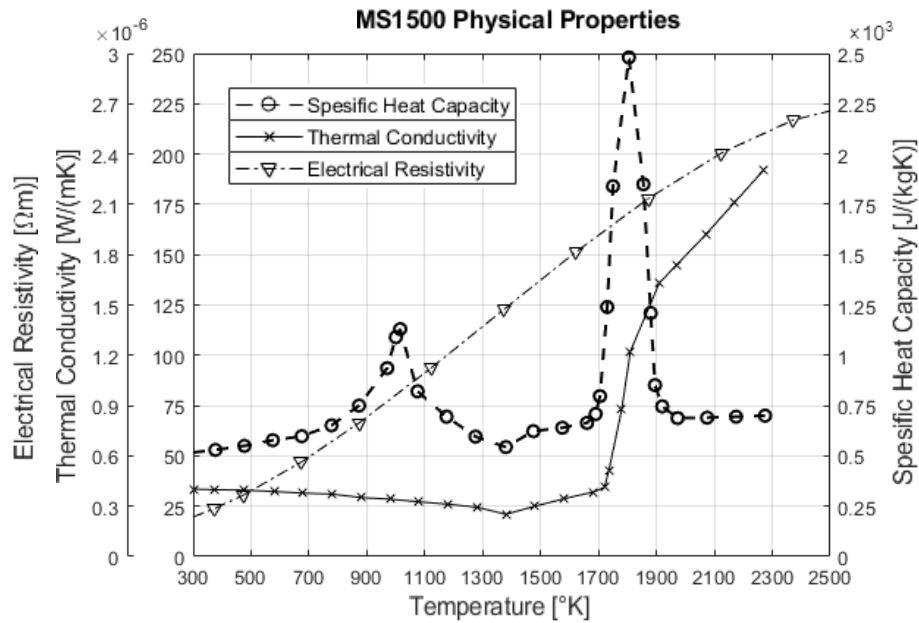


**Figure 3.2.** Physical Properties of MS1500 (See Appendix 2 for tabular values)

As stated in the previous section, the advantage of utilizing the axisymmetric geometry in the RSW process has been acknowledged. The process has been modelled with two workpiece MS1500 sheets, each with a thickness of 1.2mm, as deformable meshed bodies. The electrodes, modelled as non-deformable geometric bodies using 2 arc curves, are regulated by a control node. Electrode caps are modelled per Type G -40mm spherical segment tip radius according to ISO5821. Radius of the workpieces modelled as 7mm. Element size on the probable nugget formation area is 0.1mm, gradually increasing the element size beyond the nugget area. At the far end of the radius, the element size becomes 0.26mm. Model consists of 1440 elements (each workpiece has 720 elements) and 1586 nodes +1 control node. Figure 3.3. shows the general view of the created model. The four-node axisymmetric isoparametric quadrilateral element with full integration (MSC Marc library element type 10) is used to model the workpieces. Type 10 element uses bilinear interpolation functions, so the strains tend to be constant throughout the element which results in a poor representation of shear behaviour. Since its lower order element than the type 28 (8 node axisymmetric element), fine mesh is required to accurate representation of strain fields. But the type 10 element is preferred in contact analyses. Due to RSW simulation model is electro-thermo-mechanical coupled, with the selection of type 10 element, software uses on the background type 40 elements which associated heat transfer element type. It's also capable of joule heating calculations [23].

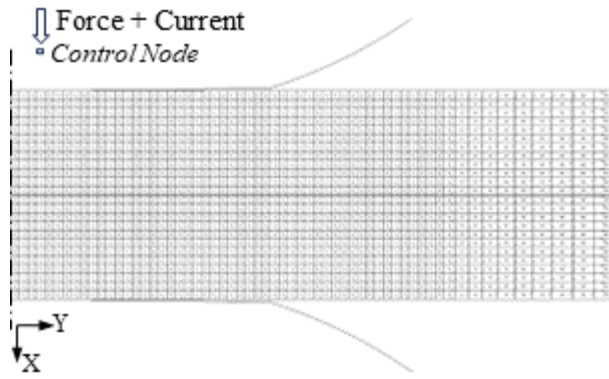


**Figure 3.3.** Finite Element Model of RSW Process

In an RSW process that performed with alternating current, process control parameters on heating are the maximum current and the cycle count. Also, the other controlled process parameter is the applied force on workpieces. There are three stages during the application of force, squeeze time, weld time, hold time. Electric current flows on workpieces during the weld time when the force is maximum. Figure 3.4. shows the 10-cycle process flow with normalised force and current. In this work, simulation of RSW performed with 10-12 cycles and a maximum AC current of 8-10 kA and the maximum force of 3-4 kN. Since the solidification was mostly complete, its assumed that 0.4 seconds is sufficient for analysis.

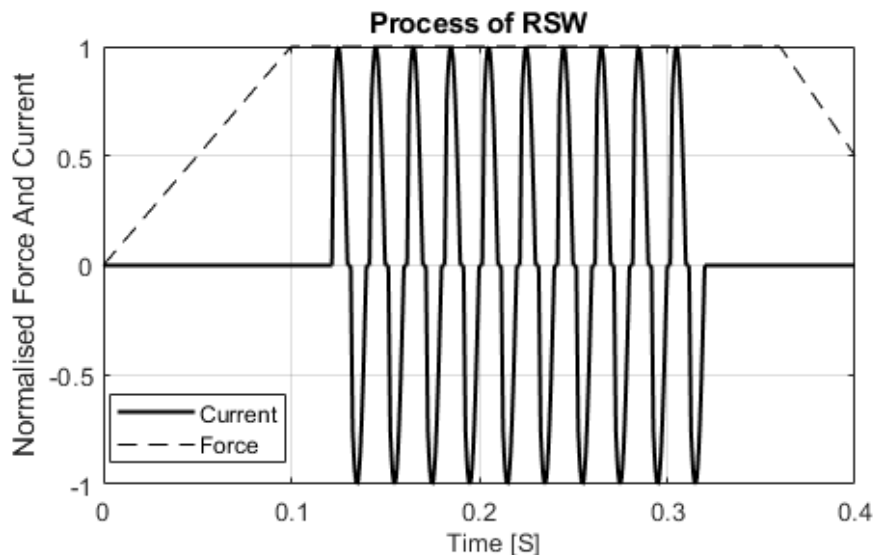


**Figure 3.4.** Process parameters (Force and 10 Cycle Current w.r.t. Time)

Source of AC current follows a sine wave. While RSW process machines apply the current received from the source to the workpieces, they cannot apply AC as smooth sine wave due to the electrical components used to control the current parameters. At the first moment when the current received from the source begins to differ from zero, no current flows on the workpieces instantly. After some delay, an electric current is applied to electrodes changing to a slope that captures the sine wave coming from the source. Figure 3.5. shows 1 cycle of the 50 Hz AC profile applied on the workpieces.

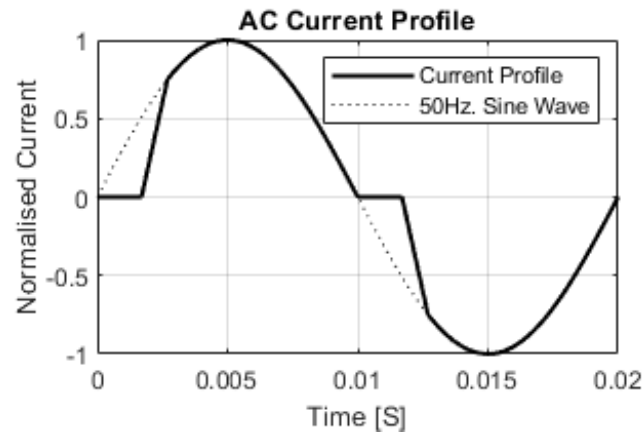


**Figure 3.5.** AC Current Application on RSW

To fully define real physics to the numerical analysis model, electrical and thermal contact properties are defined. Both the contact heat and contact electrical conductivity coefficients between the copper electrode - steel workpiece and between steel workpiece-steel workpiece are temperature and normal force dependent. Also, the surface roughness has effects on these values. But it's too complicated to define these parameters to calculations like real physics. Temperature dependent electrical contact conductivity have significantly more effect than temperature dependent heat transfer coefficient on the RSW process. In order to simplify analysis calculations and reduce the amount of input data, the contact heat transfer coefficient is assumed to be constant in all temperatures, and the electrical contact conductivity coefficient is defined as temperature dependent. Figure 3.6 shows the change of electrical contact conductivity with respect to temperature. Both coefficients are defined independent of the normal force. Contact heat transfer coefficients and the electric contact conductivity coefficients shown in Table 3.4.

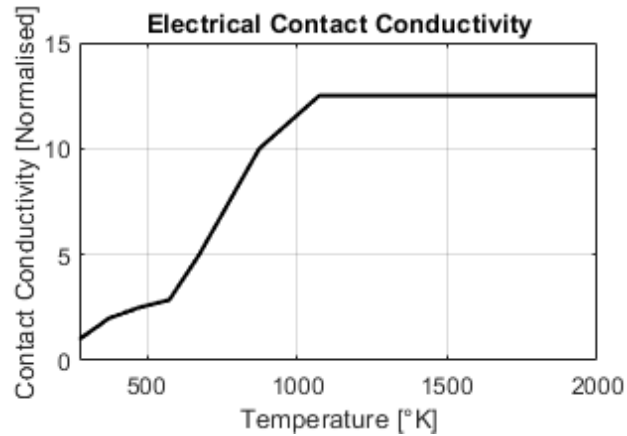


**Figure 3.6.** Change of Contact Electrical Conductivity w.r.t Temperature (See Appendix 2 for tabular values)

**Table 3.4.** Contact Properties Defined on Model

Contact Property	SI Based	Marc Units
Thermal contact conductivity (Conductance) between workpieces (Steel-Steel)	5000 [W / (m <sup>2</sup> °K)]	5 [mW / (mm <sup>2</sup> °K)]
Thermal contact conductivity (Conductance) between electrode and workpiece (Copper-Steel)	20000 [W / (m <sup>2</sup> °K)]	20 [mW / (mm <sup>2</sup> °K)]
Electrical contact conductivity between workpieces (Steel-Steel) *	2*10 <sup>8</sup> [1 / (Ω m <sup>2</sup> )]	0.2 [1 / (mΩ mm <sup>2</sup> )]
Electrical Contact Conductivity between electrode and workpieces (Copper-Steel) *	5*10 <sup>9</sup> [1 / (Ω m <sup>2</sup> )]	5 [1 / (mΩ mm <sup>2</sup> )]

\*Electrical contact conductivity data is temperature dependent and Table values are factor of data shown on Figure 3.6. (See Appendix 2 for tabular data)

There are essential boundary conditions defined to the FEA model to fully construct the model for RSW process. Initial temperature for all nodes is 298°K. As the electrodes created with non-deformable geometric elements, they are rigid, non-movable, 0 electric potential and have constant temperature by definition except controlled. First electrode (at negative x axis) controlled by a node and the required pressure for welding is provided by the force applied to the control node with a factor of 3400 N to the profile shown in Figure 3.4. The current is also applied to same electrode with the control node with a factor of 8000 A to the current profile shown in Figure 3.4. Axisymmetric boundary conditions are applied to all nodes by the program.

Main cooling mechanism in RSW is the conduction caused by contact heat transfer between the electrodes and the workpieces. Although air convection helps to the workpieces cool down, its effect on temperature remains relatively very low due to free convection (not forced), small heat transfer area to the surroundings, and the short time of interest for the simulation. Since the temperature changes caused by air convection were below 1%, air convection neglected in models to simplify the FEA model.

## 4. RESULTS AND DISCUSSION

The model described on previous section created with the Mentat software which is the pre-post processor unit and solved by Marc software. Nugget formation observed with coloured temperature map and compared with the experimental results for 4,6,8,10 cycle.

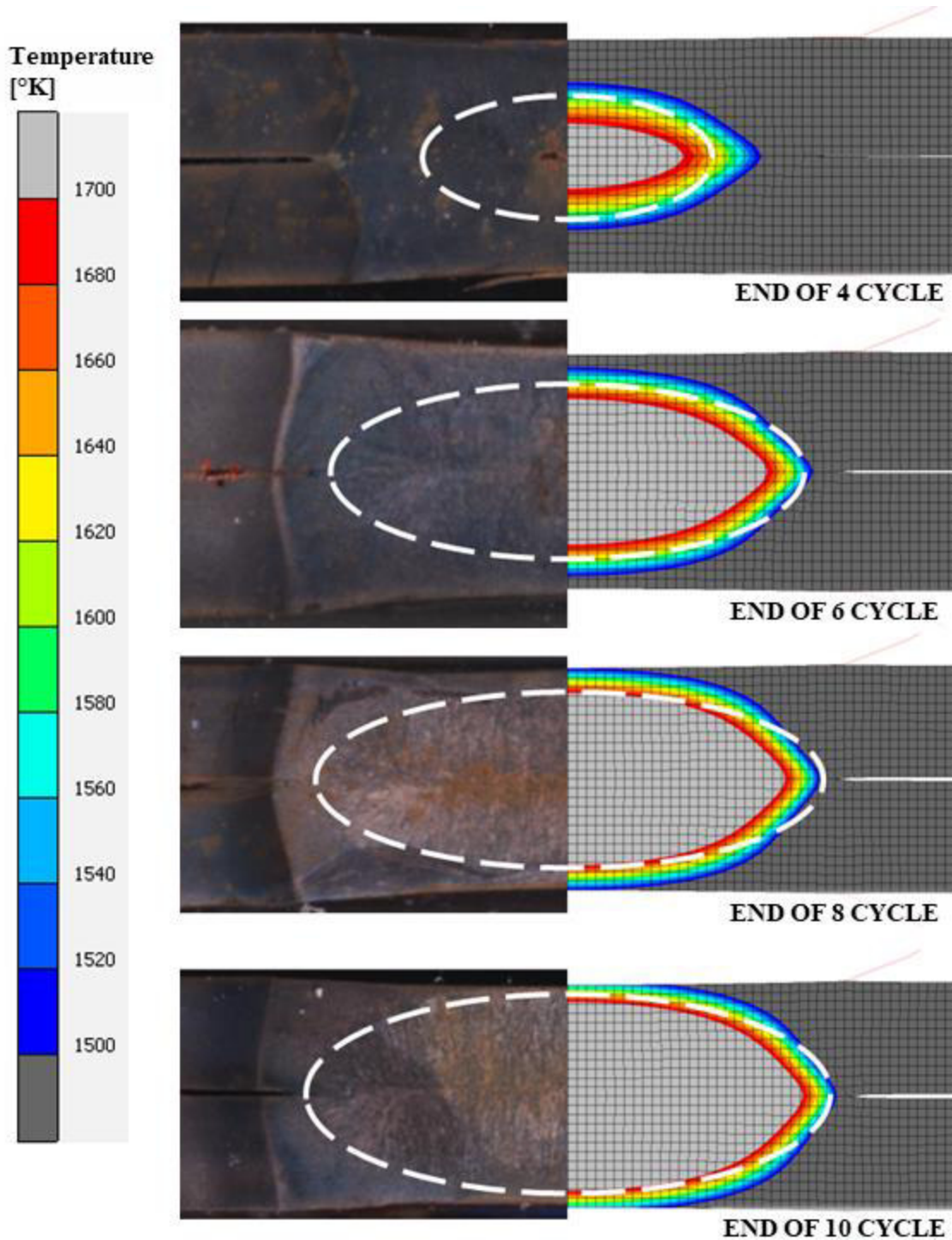


**Figure 4.1.** Comparison of Experimental and FEA Results of RSW Process with 8 kA Current and 3.4 kN of Force

In the Figure 4.1. light grey colour represents the zone above 1700 K where the workpieces molten. Nugget diameter and height comparison are shown in Table 4.1.

**Table 4.1.** Nugget dimensions of test samples and FEA results

CYCLE	Nugget	Test Sample	FEA Model	Relative Error %
End of 4 Cycle	Height	1.33	0.69	48.12
	Width	2.86	2.82	1.39
End of 6 Cycle	Height	1.52	1.49	1.97
	Width	4.09	4.25	3.91
End of 8 Cycle	Height	1.88	1.9	1.06
	Width	5.01	5.06	0.99
End of 10 Cycle	Height	2.08	2.1	0.96
	Width	5.53	5.45	1.44

Maximum relative error occurred after 4th cycle as seen in Table 4.1. It is difficult to visually distinguish the molten region from the heat affected region of the test sample on which 4 cycles of current has been applied. Even though the nugget width is approximately the same, the big difference is in nugget height. There are possible reasons for that. These early cycles in the process result in extremely rapid temperature changes in the work pieces. The heat source of the RSW is joule heating. Since the current is applied with same profile along the welding, the total resistance of the work pieces and the contact surfaces determines the total heat generated. Additionally, the specific heat capacity of the work pieces was modelled as gradually increasing, starting from the lowest value at room temperature, until temperatures above 1000 K at which is the phase change occurs (see Figure 3.2.). Therefore, the temperature change is greatest at these initial temperatures as a result of high heat generation and the low specific heat capacity. This causes possible deviations in the results of models that are not identical to reality. Since the width of the nugget depends mostly on the heat generated by the contact surface of work pieces, the relative error is lower than the height.

Except for the nugget height error in the 4th cycle results, the reasons for which are explained, the nugget sizes of the experiment samples and the observed in the FEM model results are very close to each other.

In addition to nugget size, FEM model results also facilitate the prediction of expulsion, which is an external discontinuity of RSW, by indicating the distance between molten region and the boundaries of the closed material region. To observe the interfacial expulsion experimentally, test samples in which the RSW process was applied at 9-10 kA currents and certain predetermined cycles were examined.

In order to examine the test samples for interfacial expulsion, the welded parts were loaded into the tensile testing machine in the shear direction of weld nugget as shown in Figure 4.2.

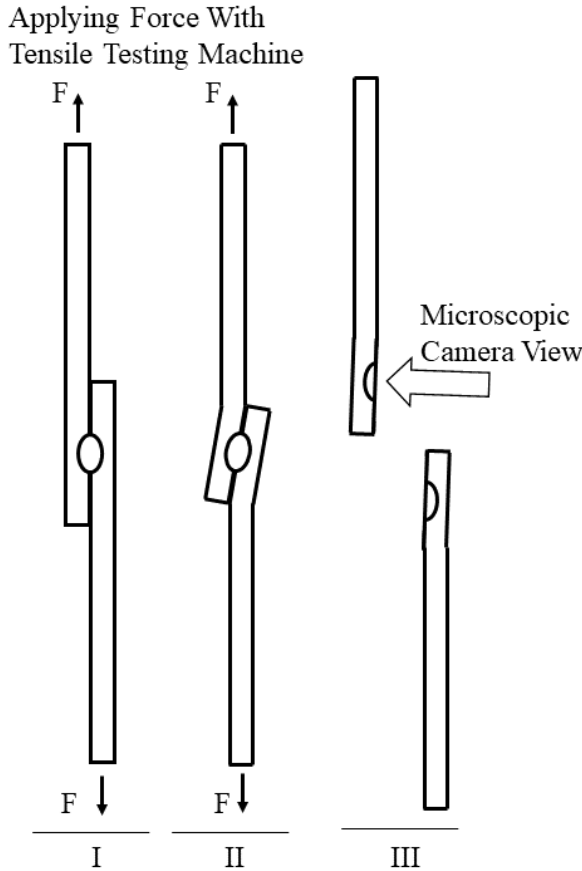


**Figure 4.2.** Schematic Representation of the Experiment of Shear Breaking on Welded Joint to Investigate the Expulsion Occurrence.

To investigate whether expulsion occurred in the test samples broken off from the welding area, digitally calibrated scale photographs were taken with a microscopic camera and matched with the FEM results as shown in Figures 4.3 and 4.4.

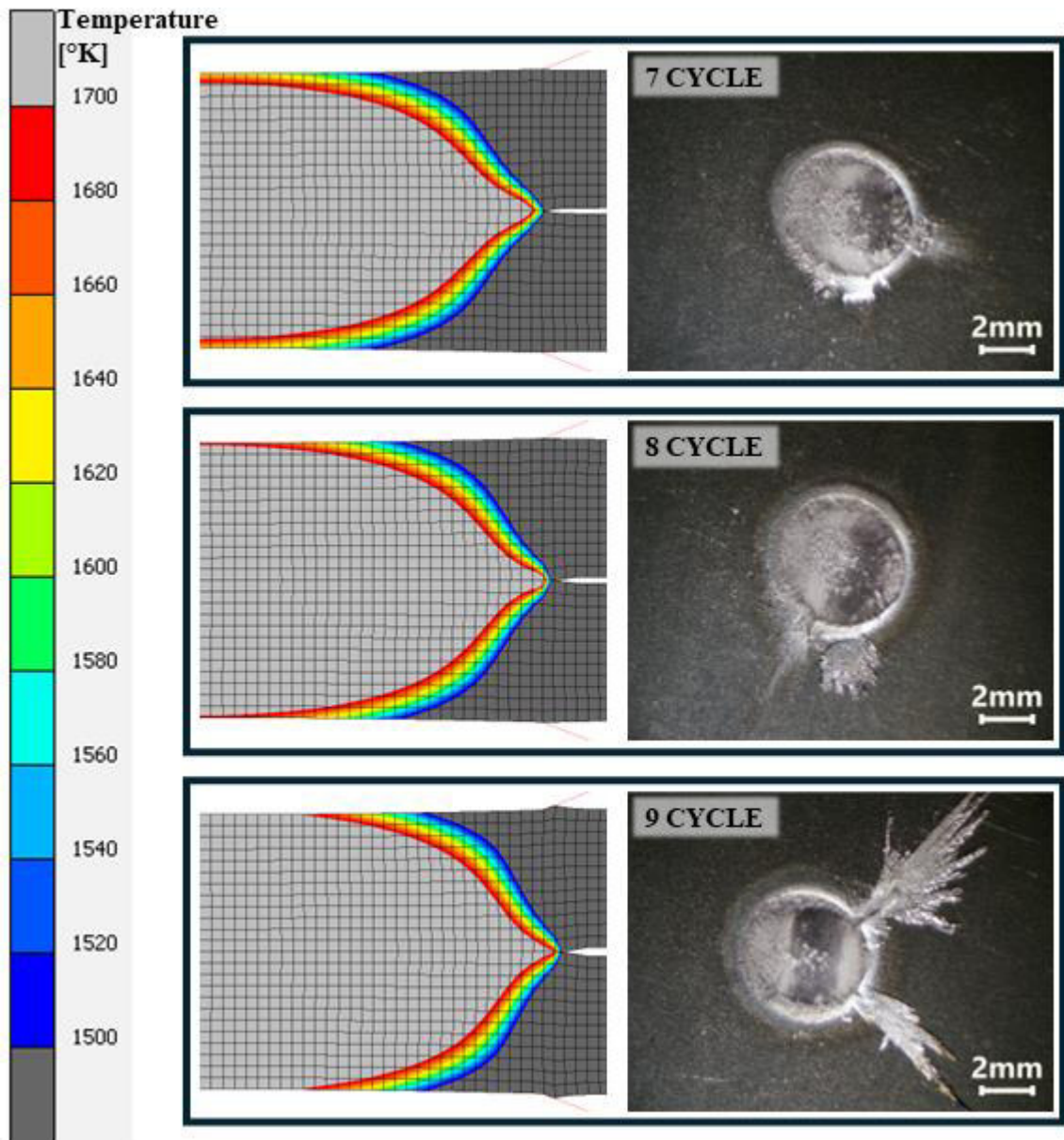


**Figure 4.3.** Expulsion Comparison of Experimental and FEA Results of RSW process with 9 kA current and 3.4 kN of force

FEM results show that after 9 cycles of 9kA current application, the molten zone reaches to the edge of the closed material region between work pieces which results in expulsion. But before 9 cycles, molten zone is very close to boundary, so it's complicated to predict expulsion occurrence. As can be seen in Figure 4.3., minimal expulsion occurred 7<sup>th</sup> and 8<sup>th</sup> cycle, but noticeable expulsion occurred after 9 cycle of current. For 10kA maximum current application, minimal expulsion occurred after 4<sup>th</sup> and 5<sup>th</sup> cycles, and noticeable expulsion observed after 6<sup>th</sup> cycles. Molten zone is very close to closed material boundary both on 4<sup>th</sup> and 5<sup>th</sup> cycles for 10kA and reaches to the edge on 6<sup>th</sup> cycle. The matched FEM result images are not taken after the stated cycle, instead 16-24 millisecond (8-12

increment for model) before the cycle completion because of the maximum temperature as well as the maximum molten zone appears.

The FEM results also indicate the expulsion at the electrode and workpiece interface which does not have harmful effects on the weld, but it decreases the electrode life. During the welding process of test samples for expulsion investigations, expulsion occurred on the sheet and electrode for every weld made but it was significantly more visible at 9 cycle application for 9kA current and 6 cycle application for 10kA.

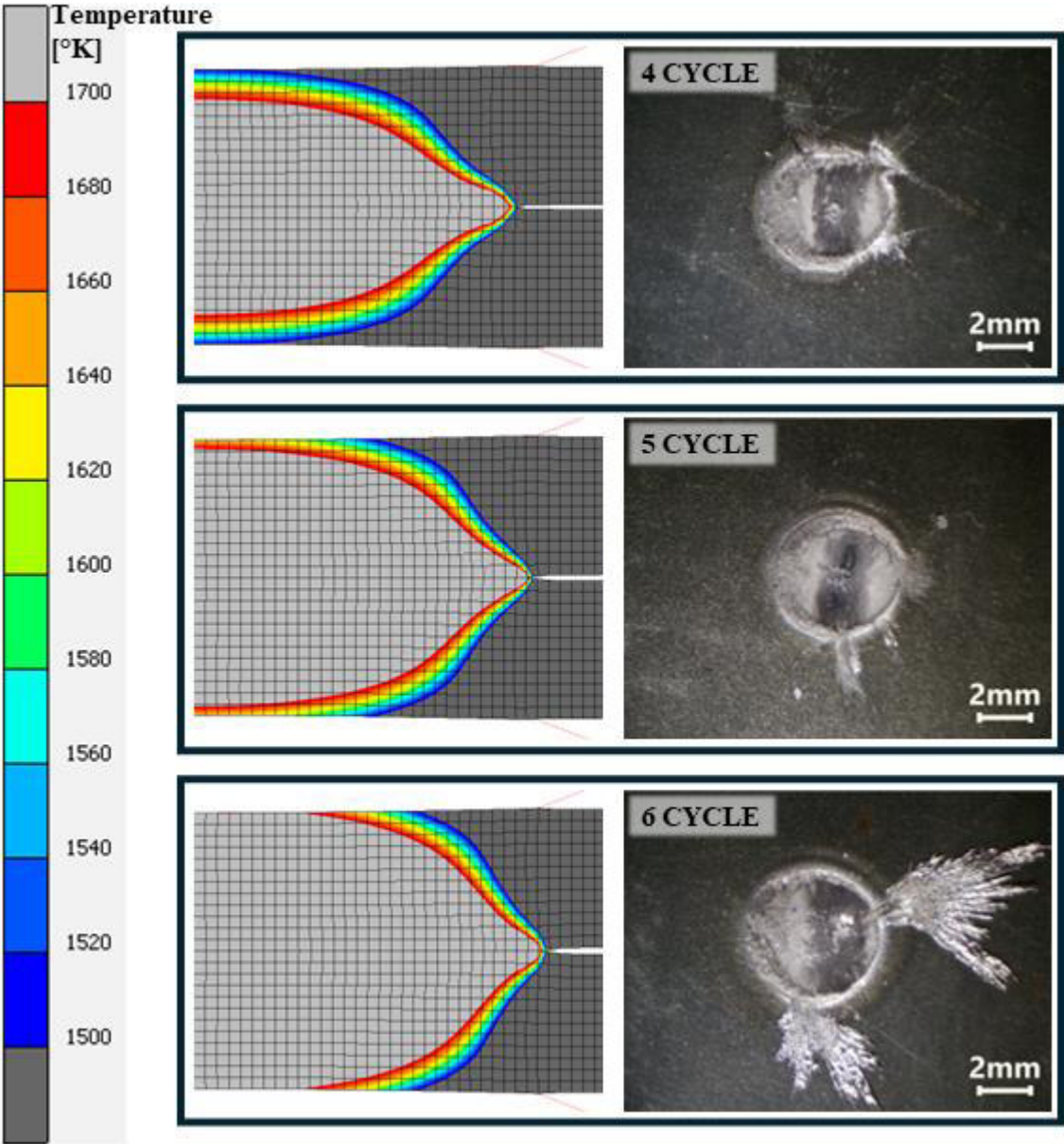


**Figure 4.4.** Expulsion Comparison of Experimental and FEA Results of RSW process with 10 kA current and 3.4 kN of force

The steel microstructure and hence its mechanical properties are highly dependent on heat treatment. Since there are very high temperature changes in a very short time interval during RSW operation, it has a great effect on these properties. The simulation has the temperature vs. time output, so the microstructure of the workpieces after RSW process can be examined. For this purpose, some changes made on the analysis parameters. The job duration for holding time of RSW extended from 0.4s to 0.92s to observe temperatures down to martensite start temperature on welded sheets. Since the simulation cannot carry out the fuse bonds, as the weld nugget cools down, the steel workpiece bodies separate, and they regain their defined properties at low temperatures. This causes misleading contact surfaces for heat transfer between the electrode and workpieces. In order not to observe unrealistic temperatures due to incorrect heat transfer rates of contact surfaces, the squeezing force parameter kept constant at its maximum value 3.4kN until the end of the analysis. The graph of temperatures at the nodes defined in Figure 4.5. during the electric current application phase of the RSW process is shown in Figure 4.6. The temperature changes after the application of current in the RSW process on the defined nodes shown in Figure 4.7.

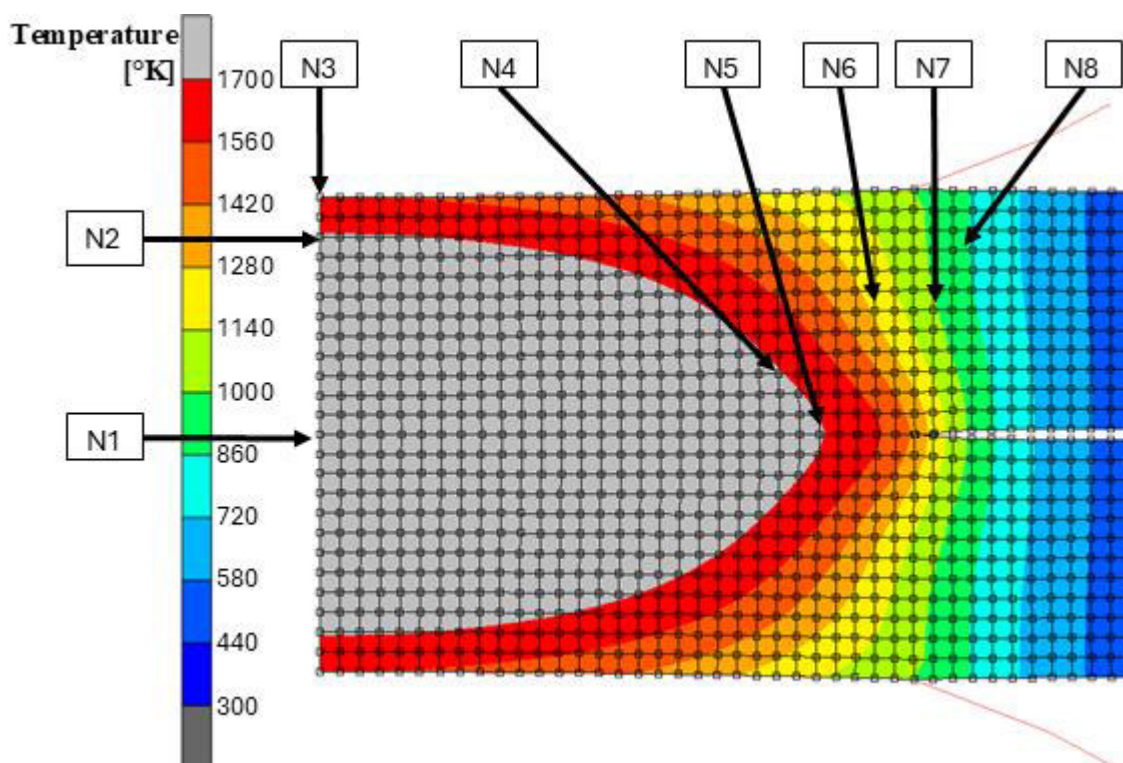


**Figure 4.5.** Identification of nodes whose temperatures are examined in the analysis

Temperature of the nodes which close to nugget area, increases in an oscillated fashion because of the alternating current. The local peaks of the temperature graph represent half cycle of current application. One complete cycle of current time, 20 milliseconds since the alternating current frequency is 50Hz, marked with the gridlines in the Figure 4.6. Nodes N2 and N4 are located on the borderline of the nugget so they slightly exceed the melting temperature. Node N1 on the center of the nugget and the rate of increase in temperature decreases after melting temperature because the latent heat modelled as sudden increase in specific heat capacity. Temperature of the nodes N6, N7 and N8 do not increase oscillatorily, but instead increases almost in a straight line. Because they are located outside the current flow lines which starts from one electrode passes through contact surface between steel workpieces and ends on the other electrode. The absence of current passing them means that heating does not occur with joule heating. The increase in their temperatures is due to heat transferred from other nodes that are heated by Joule heating, a result of the material thermal conductivity.

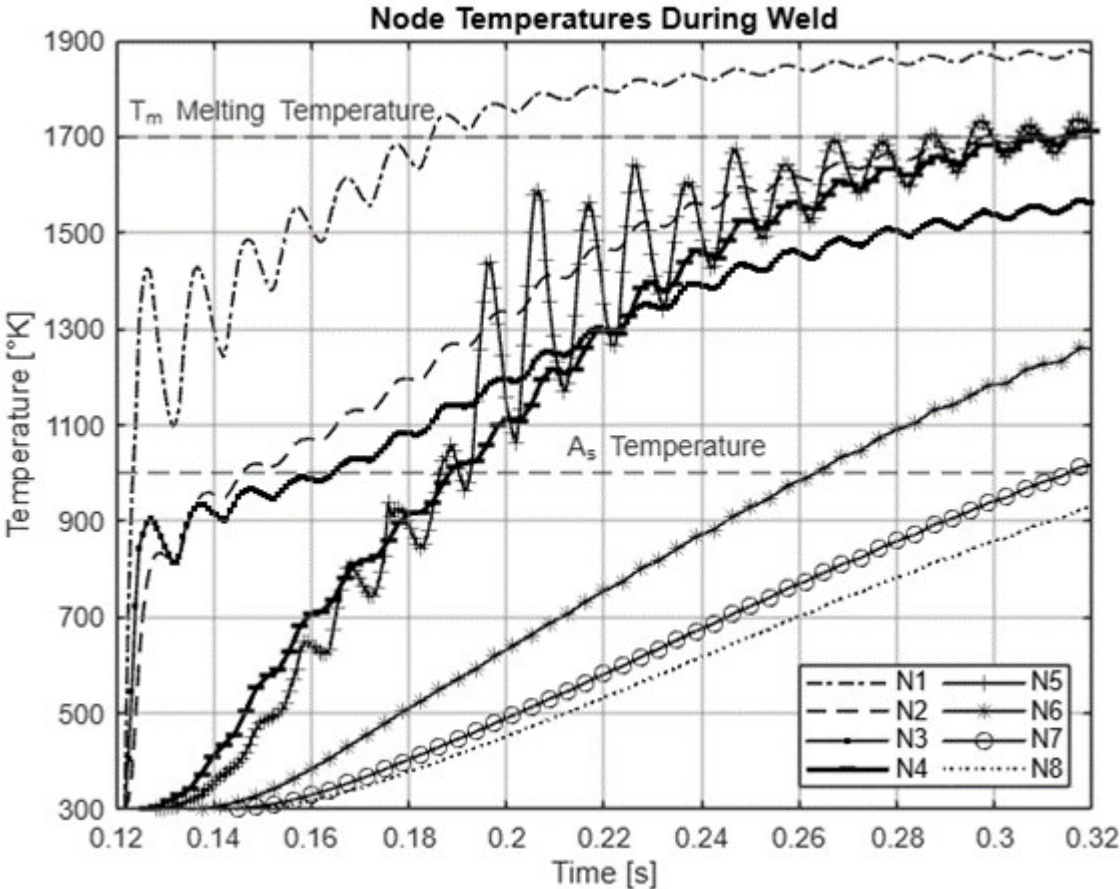


**Figure 4.6.** Temperature data of the selected nodes during current application in the analysis

The joule heating effect increase temperatures rapidly on the beginning of the RSW process, afterwards it slows down because the total resistance of the system has the highest value in early cycles because of the very high contact resistance. As the temperature increases, the material resistance become dominant but total resistance does not exceed its initial value. The contact resistance decreases because of the increase in contact surface and temperature dependent defined contact conductivity parameters.

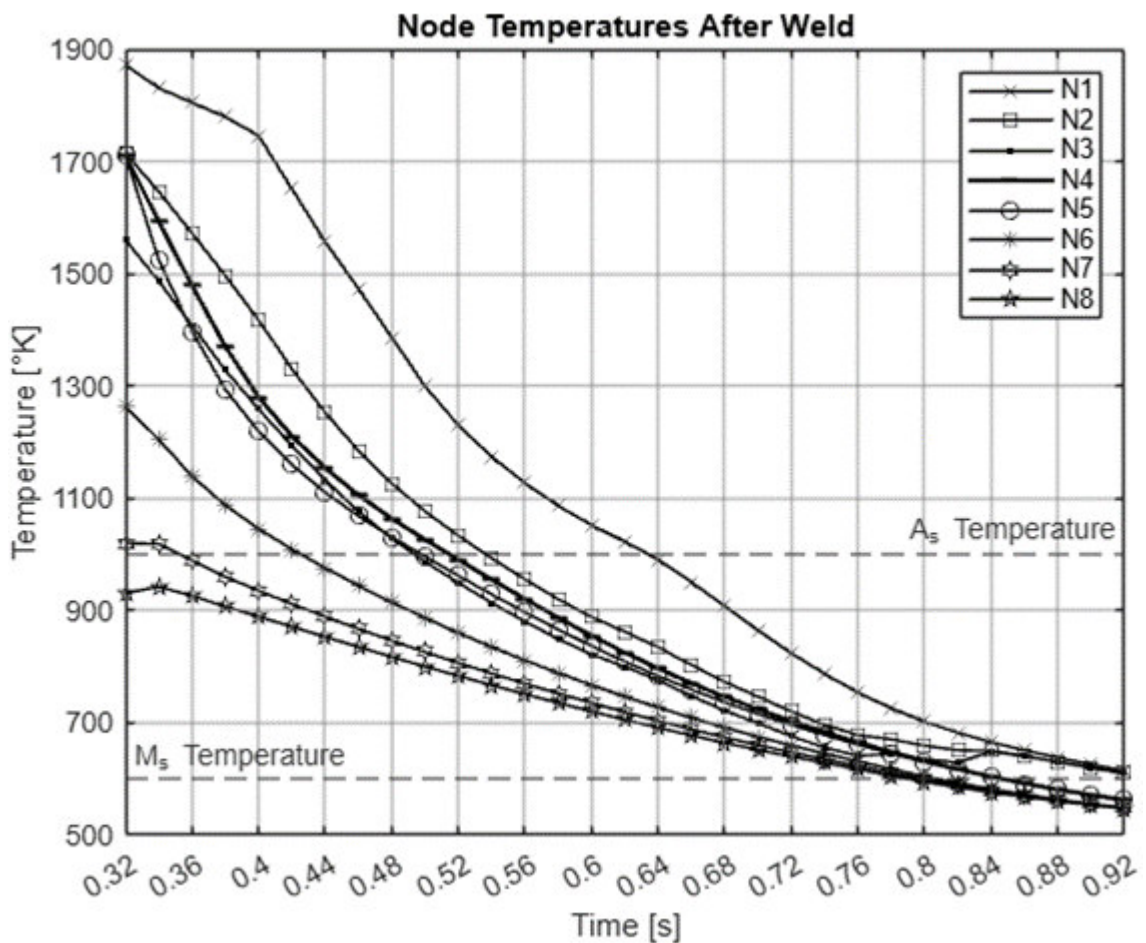


**Figure 4.7.** Temperature data of the selected nodes after current application in the analysis

The temperature-time graph shows that the cooling rates relatively too high than the conventional heat treatment processes. Its because the high cooling effect of the copper electrodes and the mass to be cooled is very small. N1 node is on the centre of the nugget, so its temperature is higher than the melting point. Temperature change rate of the N1 node is relatively slow at the beginning of cooling, because the latent heat modelled in

the analysis as high specific heat capacity shown in Figure 3.2. Nodes N7 and N8 are the farthest selected nodes to the nugget, so they initially heat up for a short time due to the heat transfer from the high temperature nugget to the surrounding material. All nodes start to cool down 10ms after current application at  $t=0.33s$ . Austenite transformation begins at  $T=1000^{\circ}K$  which shown as  $A_s$  on Figure 4.6. Temperature change rate slows down at  $A_s$  limit for a short period because the austenite transformation phase is modelled as specific heat capacity increase in the analysis. Afterward the cooling rate slows down as the temperature of the steel work pieces approaches to the temperature of cold copper electrodes which modelled as constant at room temperature.

At  $600^{\circ}K$  ( $M_s$  Temperature) martensitic transformation starts, and the solid-state phase transformation requires high cooling rate. In the results of the analysis, temperature change rates are rapid enough to form martensite microstructure shown in Table 4.2.

**Table 4.2.** Temperature change rate on different time intervals of selected nodes

Time Definition		Cooling Rate ( $^{\circ}K/s$ )							
Time Interval	$\Delta$ Time [s]	N1	N2	N3	N4	N5	N6	N7	N8
0.33-0.48	0.15	3072	3703	3303	3942	3812	2176	1216	843
0.48-0.80	0.32	2139	1459	1228	1349	1253	969	770	695
0.80-0.92	0.12	728	409	211	579	560	472	424	400

Further data not available on the analysis but can be assumed constant cooling rate after martensitic start temperature ( $M_s$ )  $600^{\circ}K$  to martensitic finish temperature ( $M_f$ ) around  $450^{\circ}K$ . Thus, by looking at the data in Table 4.2, it can be said that the solid phase of the steel in the weld nugget and its surroundings after the RSW process is martensite due to the very rapid cooling. Node N3 have lowest cooling rate in the time interval of 0.80-0.92 seconds. It's in the centre of the contact surface between the copper electrode and the steel workpiece. This makes node N3 is close to the weld nugget and have enough heat transfer to increase its temperature due to high temperature of the nugget, also it has the highest heat transfer to the electrode to decrease its temperature. The simulation results are fluctuating around the  $630-660^{\circ}K$  for the node N3 at time interval of  $t= 0.77-0.84 s$  but sampling size is not enough to show that in Figure 4.6. This is why the cooling rate of the N3 is lowest on the Table 4.2. for time interval of 0.80-0.92s.

## 5. SUMMARY AND OUTLOOK

In this thesis, the resistance spot welding process for ultra-high strength steels is investigated using electro-thermo-mechanical coupled finite element analysis and the results are compared with experiments. First, optimum weld parameters found, then the analysis results compared with the experimental test results for cycle intervals. Then the expulsion limits investigated with finite element analysis. For limit parameters found in the simulation, test coupons are welded together and broken into pieces back to examine the interfacial expulsion around the nugget. Then the holding phase of resistance spot welding is investigated to calculate temperature change rates after welding current application.

- It's found that the squeezing force of 3.4kN and maximum electrical current of 8kA with 10 cycle is optimal for the 1.2mm thick two piece of MS1500 steel. It can be said that the nugget size for optimum weld parameters were accurately predicted in the FEA simulation, with an error margin of less than 1.5% with exceptions at some cycle intervals during the current application of welding process.
- The expulsion limits were accurately predicted for higher currents. For a maximum current of 9 kA, expulsion is predicted to occur after 9 cycles, and for a maximum current of 10 kA, it is predicted to occur after 6 cycles. Test coupons welded together and broke apart to see interfacial expulsion. The test results shows that the noticeable expulsion occurs on predicted process parameters.
- Temperature change rates after current application of welding process were examined in detail. It was observed that the holding phase of process resulted in very high cooling rates on workpieces. It shows the formation of a martensitic crystalline structure around the weld nugget and its surrounding areas after the resistance spot welding process.

## 6. REFERENCES

- [1] W. Zhang, J. Xu, Advanced Lightweight Materials for Automobiles: A review, *Materials & Design*, 221 (2022). <https://doi.org/10.1016/j.matdes.2022.110994> .
- [2] E. Doruk, M. Pakdil, G. Çam, I. Durgun, U. Kumru, Otomotiv Sektöründe Direnç Nokta Kaynağı Tofaş Uygulamaları, *Kaynak Kongresi IX. Ulusal Kongre ve Sergisi*, November, 2015.
- [3] Zhang H., Senkara J., *Resistance Welding: Fundamentals and Applications*, Second Edition, CRC Press, USA, 2011, <https://doi.org/10.1201/b11752> .
- [4] N.M. Charde, Effect of Spot Welding Variables on Nugget Size and Bond Strength of 304 Austenitic Stainless Steel, *Australasian Welding Journal - Welding Technology Institute of Australia* 57 (2013) 6.
- [5] S. Keeler, M. Kimchi, P.J. Mooney, *Advanced High Strength Steels Application Guidelines*, Version 6, World Auto Steel, 2017.
- [6] D.H. Phillips, *Welding Engineering: An Introduction*, John Wiley & Sons, West Sussex UK, 2016, <https://doi.org/10.1002/9781119191407> .
- [7] G.R. Archer, Calculations for Temperature Response in Spot Welds, *Welding Journal* 39 (1960) 327s–330s.
- [8] J.A. Greenwood, Temperatures in spot welding, *British Welding Journal* 8 (1961) 316–322.
- [9] Nied A., The Finite Element Modeling of Resistance Spot Welding Process, *Welding Journal* 63 (4), (1984) 123–132.
- [10] C.L Tsai, O.A Jammal and J.C Papritan, Modeling of The Resistance Spot Welding Nugget Growth, *Welding Journal* 02, (1992) 47s-54s.
- [11] H. Eisazadeh, M. Hamed, A. Halvae, New Parametric Study of Nugget Size in Resistance Spot Welding Process Using Finite Element Method, *Materials & Design* 31 (2010) 149–157, <https://doi.org/10.1016/j.matdes.2009.06.042> .
- [12] C. V. Nielsen, K. S. Friis, W. Zhang, and N. Bay, Three-Sheet Spot Welding of Advanced High-Strength Steels, *Welding Journal*, vol. 90, (2011) 32s-40s.

- [13] W. Zheng, M. Wang, L. Kong, X. Cheng, M. Lei, Parameter Optimization of Dissimilar Resistance Spot Welding on Ultra-High Strength Hot-Stamped Steel and Mild Steel by Numerical Simulation, *Acta Metallurgica Sinica (English Lett.)* Vol. 25(6) (2012) 487–498, <https://doi.org/10.11890/1006-7191-126-487> .
- [14] Andersson O. and Melander A., Prediction and Verification of Resistance Spot Welding Results of Ultra-High Strength Steels through FE Simulations. *Modeling and Numerical Simulation of Material Science*, Vol. 5 No.1 January, (2015) 26-37, <http://dx.doi.org/10.4236/mnsms.2015.51003> .
- [15] Hong Li, Weijia Yan, Zhuoxin Li, Bober, Mariusz, Senkara J. and Yu Zhang, Numerical and Experimental Study of The Hot Cracking Phenomena in 6061/7075 Dissimilar Aluminum Alloy Resistance Spot Welding, *Journal of Manufacturing Processes*. 77. (2022) 794-808, <https://doi.org/10.1016/j.jmapro.2022.04.001> .
- [16] H. Ueda, S. Furusako, T. Okada, S. Kikuchi, Liquid Metal Embrittlement in Resistance Spot Welding (Fourth Report): - Evaluation of Liquid Metal Embrittlement Using Resistance Spot Welding FEA Simulation, *International Journal of Automotive Engineering* Vol. 11 Issue 3, (2020), 129-135, [https://doi.org/10.20485/jsaeijae.11.3\\_129](https://doi.org/10.20485/jsaeijae.11.3_129)
- [17] Wook-Sang Jeon, Ashutosh Sharma, Jae Pil Jung, Liquid Metal Embrittlement of Galvanized TRIP Steels in Resistance Spot Welding. *Metals*, Vol. 10 No 6 Article No 787 (2020), <https://doi.org/10.3390/met10060787> .
- [18] M. Jafari, A. Arayee, and J. Senkara, A Review of Finite Element Analysis (FEA) of Resistance Spot Welding (RSW), *Weld. Tech. Rev.* Vol. 88, No 2, (2016), <https://doi.org/10.26628/ps.v88i2.571> .
- [19] Yildirim, B., and Nied, H. F., Residual Stresses and Distortion in Boiler Tube Panels With Welded Overlay Cladding, *ASME. J. Pressure Vessel Technol.* November, (2004), 126(4): 426–431, <https://doi.org/10.1115/1.1804198>
- [20] Gerson Meschut, Michael Rethmeier, Combined Reports AHSS Implementation Solutions: Liquid Metal Embrittlement Study, Final Report, World Auto Steel, 2020.
- [21] Christopher Schwenk, FE-Simulation des Schweißverzugs laserstrahlgeschweißter dünner Bleche, Technical University of Berlin, Faculty V – Transport and Mechanical Systems, Berlin, 2007.

[22] ASM International Handbook Committee, Properties and Selection: Irons, Steels, and High-Performance Alloys, ASM International, **1996**.

[23] MSC Marc User Documentation Volume B , MSC.Software Corporation, **2016**.

## APPENDIX

### Appendix 1 – Marc Unit System (millimetre based)

Units used on MSC Marc:

Measurement	SI Base Units	SI Unit	Marc Base Unit (mm)	Marc Unit (mm)
Length	m		mm	
Mass	kg		t	
Temperature	K		K	
Electrical				
Current	A		A	
Time	s		s	
Area	m <sup>2</sup>		mm <sup>2</sup>	
Volume	m <sup>3</sup>		mm <sup>3</sup>	
Mass Density	kg/(m <sup>3</sup> )		t/(mm <sup>3</sup> )	
Velocity	m/s		mm/s	
Acceleration	m/(s <sup>2</sup> )		mm/(s <sup>2</sup> )	
Force	kg*m/(s <sup>2</sup> )	N	t*mm/(s <sup>2</sup> )	N
Stress	kg/(s <sup>2</sup> )*m	Pa	t/(s <sup>2</sup> )*mm	MPa
Work	kg*(m <sup>2</sup> )/(s <sup>2</sup> )	J	t*(mm <sup>2</sup> )/(s <sup>2</sup> )	mJ
Power	kg*(m <sup>2</sup> )/(s <sup>3</sup> )	W	t*(mm <sup>2</sup> )/(s <sup>3</sup> )	mW
Thermal				
Conductivity	kg*m/((s <sup>3</sup> )*K)	W/(m*K)	t*mm/((s <sup>3</sup> )*K)	mW/(mm*K)
Specific Heat	(m <sup>2</sup> )/((s <sup>2</sup> )*K)	J/(kg*K)	(mm <sup>2</sup> )/((s <sup>2</sup> )*K)	mJ/(t*K)
Electric				
Potential	kg*(m <sup>2</sup> )/(A*(s <sup>3</sup> ))	V	t*(mm <sup>2</sup> )/(A*(s <sup>3</sup> ))	mV
Electrical				
Resistance	kg*(m <sup>2</sup> )/((s <sup>3</sup> )*(A <sup>2</sup> ))	Ω	t*(mm <sup>2</sup> )/((s <sup>3</sup> )*(A <sup>2</sup> ))	mΩ
Electrical				
Resistivity	kg*(m <sup>3</sup> )/((s <sup>3</sup> )*(A <sup>2</sup> ))	ρ, Ω*m	t*(mm <sup>3</sup> )/((s <sup>3</sup> )*(A <sup>2</sup> ))	mΩ*mm
Electrical				
Conductivity	(s <sup>3</sup> )*(A <sup>2</sup> )/(kg*(m <sup>3</sup> ))	1/Ω*m	(s <sup>3</sup> )*(A <sup>2</sup> )/(t*(mm <sup>3</sup> ))	1/mΩ*mm
Heat Flux	kg/(s <sup>3</sup> )	W/(m <sup>2</sup> )	t/(s <sup>3</sup> )	mW/(mm <sup>2</sup> )

Conversion factors of units:

Measurement	SI Unit	Marc Unit (mm)	Conversion Factor
Length	m	mm	1.00E+03
Mass	kg	t	1.00E-03
Temperature	K	K	1.00E+00
Electrical Current	A	A	1.00E+00
Time	s	s	1.00E+01
Area	m <sup>2</sup>	mm <sup>2</sup>	1.00E+06
Volume	m <sup>3</sup>	mm <sup>3</sup>	1.00E+09
Mass Density	kg/(m <sup>3</sup> )	t/(mm <sup>3</sup> )	1.00E-12
Velocity	m/s	mm/s	1.00E+03
Acceleration	m/(s <sup>2</sup> )	mm/(s <sup>2</sup> )	1.00E+03
Force	N	N	1.00E+00
Stress	Pa	MPa	1.00E-06
Work	J	mJ	1.00E+03
Power	W	mW	1.00E+03
Thermal	W/(m*K)	mW/(mm*K)	1.00E+00
Spesific Heat	J/(kg*K)	mJ/(t*K)	1.00E+06
Electric Potential	V	mV	1.00E+03
Electrical Resistance	Ω	mΩ	1.00E+03
Electrical Resistivity	ρ , Ω*m	mΩ*mm	1.00E+06
Electrical	1/Ω*m	1/mΩ*mm	1.00E-06
Heat Flux	W/(m <sup>2</sup> )	mW/(mm <sup>2</sup> )	1.00E-03

## Appendix 2 – Material Properties of MS1500 and Contact Parameters

Elastic Modulus (Young’s Modulus) of the defined material in the model:

Temperature [°K]	Young’s Modulus [GPa]	Young’s Modulus [MPa]*
273	211	211000
365	211	211000
460	211	211000
555	191	191000
650	170	170000
750	146	146000
840	120	120000
935	75	75000
1035	30.5	30500
1125	5.65	5650
1415	2.60	2600

\*: Unit used in MSC Marc “Milimeter” based system.

Thermal Conductivity of the defined material in the model:

Temperature [°K]	Thermal Conductivity [W/m°K]/ [mW/mm°K]*
300	33.5
375	33.2
475	33
580	32.3
680	31.5
780	31
880	29.3
980	28.5
1080	27.2
1180	26
1280	24.5
1380	21
1480	25
1580	28.7
1680	32
1720	34.3
1735	42.3
1780	73
1810	102
1910	136
1970	145
2070	160
2170	176
2270	192

\*: Unit used in MSC Marc “Milimeter” based system. SI system conversion factor is 1.

Yield Strength of the defined material in the model:

Temperature [°K]	Yield Strength [MPa]
273	1450
300	1450
1000	36.25
3000	29

Specific heat capacity of the defined material in the model:

Temperature [°K]	Specific Heat Capacity [J/(kg°K)]	Specific Heat Capacity [mJ/(t°K)] *
298	5.17E+02	5.17E+08
377	5.30E+02	5.30E+08
477	5.50E+02	5.50E+08
575	5.78E+02	5.78E+08
675	5.98E+02	5.98E+08
778	6.52E+02	6.52E+08
873	7.50E+02	7.50E+08
970	9.36E+02	9.36E+08
1000	1.09E+03	1.09E+09
1015	1.13E+03	1.13E+09
1075	8.21E+02	8.21E+08
1175	6.95E+02	6.95E+08
1275	5.96E+02	5.96E+08
1380	5.44E+02	5.44E+08
1475	6.23E+02	6.23E+08
1575	6.40E+02	6.40E+08
1660	6.64E+02	6.64E+08
1690	7.08E+02	7.08E+08
1705	7.97E+02	7.97E+08
1730	1.24E+03	1.24E+09
1750	1.84E+03	1.84E+09
1805	2.48E+03	2.48E+09
1855	1.85E+03	1.85E+09
1880	1.21E+03	1.21E+09
1895	8.52E+02	8.52E+08
1920	7.46E+02	7.46E+08
1973	6.88E+02	6.88E+08
2075	6.90E+02	6.90E+08
2175	6.95E+02	6.95E+08
2275	7.00E+02	7.00E+08

\*: Unit used in MSC Marc “Milimeter” based system.

Electrical Resistivity of the defined material in the model:

<b>Temperature [°K]</b>	<b>Electrical Resistivity [ohm*m]</b>	<b>Electrical Resistivity [mohm*mm]</b>
293	2.32E-07	0.2316
373	2.86E-07	0.2856
473	3.66E-07	0.366
673	5.63E-07	0.5628
873	7.97E-07	0.7968
1123	1.13E-06	1.1256
1373	1.47E-06	1.4736
1623	1.82E-06	1.818
1873	2.14E-06	2.136
2123	2.40E-06	2.4048
2373	2.60E-06	2.604
2623	2.71E-06	2.7084

\*: Unit used in MSC Marc “Milimeter” based system.

Contact Electrical Resistivity (Normalised) between electrode-sheet and sheet-sheet

<b>Temperature [°K]</b>	<b>Contact Electrical Resistivity</b>
273	1
373	2
473	2,50
573	2,86
673	5
873	10
1073	12,5
1273	12,5